Contents lists available at ScienceDirect

Materials Today Bio

Adsorption of SARS CoV-2 spike proteins on various functionalized surfaces correlates with the high transmissibility of Delta and Omicron variants

Daniela Dobrynin [a], Iryna Polishchuk [a], Lotan Portal [a], Ivan Zlotver [b], Alejandro Sosnik [b,**], Boaz Pokroy [a,*]

[a] Bio-Inspired Surface Engineering and Biomineralization Lab, Department of Materials Science and Engineering, Technion – Israel Institute of Technology, 32000, Haifa, Israel
[b] Laboratory of Pharmaceutical Nanomaterials Science, Department of Materials Science and Engineering, Technion – Israel Institute of Technology, 32000, Haifa, Israel

ARTICLE INFO

ABSTRACT

The SARS-CoV-2 virus emerged at the end of 2019 and rapidly developed several mutated variants, specifically the Delta and Omicron, which demonstrate higher transmissibility and escalating infection cases worldwide. The dominant transmission pathway of this virus is via human-to-human contact and aerosols which once inhaled interact with the mucosal tissue, but another possible route is through contact with surfaces contaminated with SARS-CoV-2, often exhibiting long-term survival. Here we compare the adsorption capacities of the S1 and S2 subunits of the spike (S) protein from the original variant to that of the S1 subunit from the Delta and Omicron variants on self-assembled monolayers by Quartz Crystal Microbalance. The results clearly show a significant difference in adsorption capacity between the different variants, as well as between the S1 and S2 subunits. Overall, our study demonstrates that while the Omicron variant is able to adsorb much more successfully than the Delta, both variants show enhanced adsorption capacity than that of the original strain. We also examined the influence of pH conditions on the adsorption ability of the S1 subunit and found that adsorption was strongest at pH 7.4, which is the physiological pH. The main conclusion of this study is that there is a strong correlation between the adsorption capacity and the transmissibility of the various SARS-CoV-2 variants.

1. Introduction

Coronaviruses are a highly diverse family of positive single-stranded RNA viruses, whose genome is packed within a capsid formed by the nucleocapsid (N) protein and surrounded by an envelope formed by the envelope (E) protein [1,2]. Three structural proteins are associated with the envelope, namely the membrane (M) protein and E that assemble the virus and the spike (S) protein that mediates virus entry into a host cell.

In December 2019, a new human coronavirus, Severe Acute Respiratory Syndrome coronavirus 2 (SARS-CoV-2) which causes the coronavirus disease (COVID-19), was identified and declared a global pandemic by the World Health Organization (WHO) [3,4]. Since then, the virus has continued to mutate and spread across the world, with almost 475 million cases and more than 6.1 million deaths between January 2020 and March 2022.

The spike of SARS-CoV-2 is a homotrimer glycoprotein named S protein composed of two subunits S1 and S2 that is responsible for the

attachment and entry of the virus into the host cell via the host membrane receptor, angiotensin-converting enzyme 2 (ACE2) [5,6]. The ACE2 receptor is ubiquitous and is distributed mainly in the lungs, heart, intestine, kidney and eyes [7]. A scheme of the general structure of SARS-CoV-2 and its attachment and entry into the host cell are presented in Fig. 1A. The S1 subunit consists of two domains, N- and C-terminal, and it binds the ACE2 receptor through the receptor-binding domain (RBD) located on the N-terminal domain. The S2 subunit, composed of five domains enclosing mainly hydrophobic amino acids, plays a key role in fusion of the virus with the host cell membrane [8,9]. Such fusion and cell entry are both activated by transmembrane protease serine 2 (TMPRSS2), which cleaves the S protein in S1/S2 and S2 sites [6,10,11]. The transmissibility of respiratory viruses is governed by their infectivity, the contagiousness of the infected individual, the susceptibility of the exposed individual, the contact patterns between them, and environmental factors [12]. Therefore, any mutation in the S protein, and especially in its RBD, can affect the virus's infectivity and consequently its
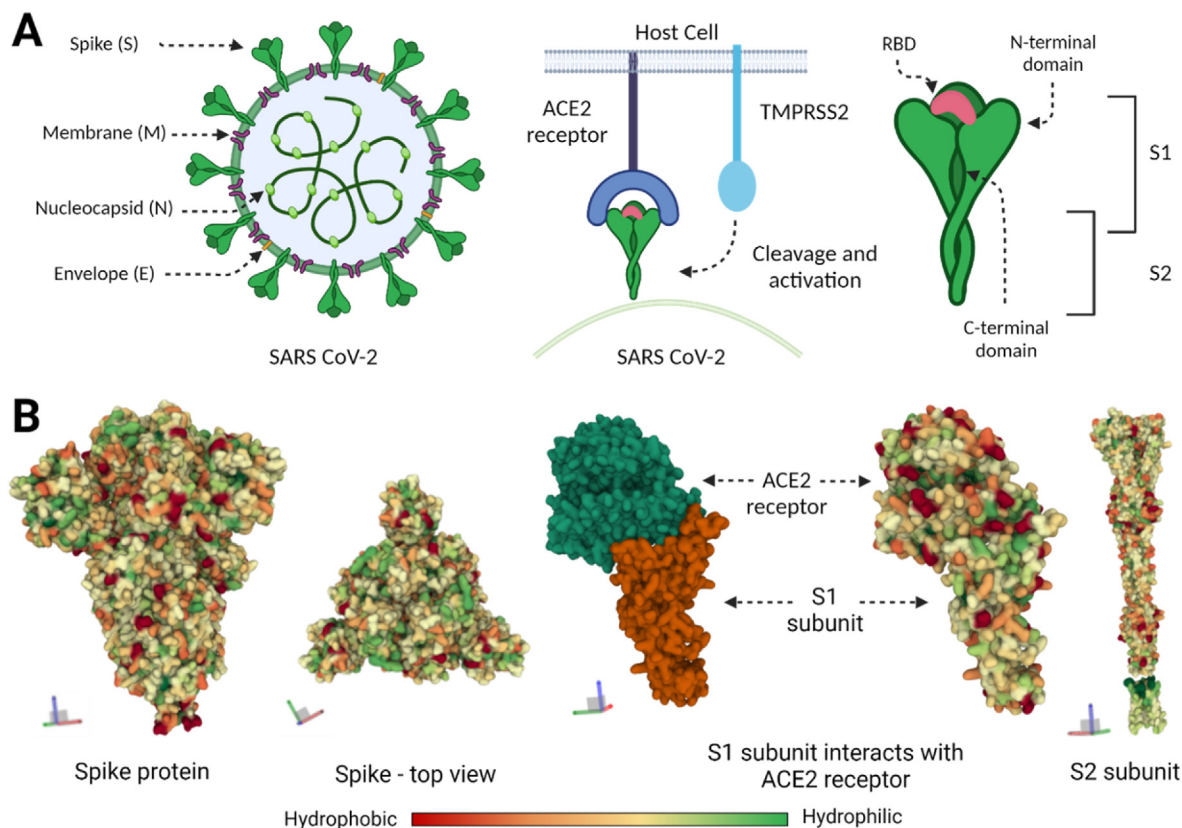
Fig. 1. (A) Schematic presentation of SARS-CoV-2 and Spike (S) protein attachment to the ACE2 receptor. (B) 3D structure of the S protein and presentation of the hydrophilicity-hydrophobicity of the surface (left to right): whole S protein and the top view, which shows S1 subunit (RCSB PDB: 6ZWV), the interaction between S1 monomer and ACE2 receptor (RCSB PDB: 7A91) and the post-fusion S2 subunit (RCSB PDB: 7E9T). Adapted from "SARS-CoV-2 structure", by BioRender.com (2022). Retrieved from https://app.biorender.com/biorender-templates.

transmissibility. Recently yet another variant has been identified, namely the B.1.1.529 or Omicron variant, which exhibits 39 mutations in its S protein, including 15 in the RBD [13,14]. As a consequence, this new variant has even higher transmissibility characteristics than the Alpha, Beta, Gamma and the especially aggressive Delta, and has therefore become the dominant variant globally [15,16].

One of the possible pathways by which SARS-CoV-2 spreads and transmits to humans is through contact with solid surfaces contaminated with the virus [17–23]. For instance, the virus has been shown to survive on surfaces such as plastics, fabrics, metals and glass, from minutes up to days [19,24]. Survival of the virus depends on the environmental conditions such as temperature [25–27], humidity [27], and exposure to light [28,29]. Lately some doubts have been expressed about the ability of SARS-CoV-2 to infect humans via surfaces, but the issue is still under scientific debate and new scientific evidence suggests that even if it is not the main transmission pathway, it could still contribute to increase the morbidity [30].

The primary route for SARS-CoV-2 to transmit is through aerosols from the infected person that spread in the air we breathe [31]. The respiratory tract is a mucosal tissue and coated with mucus and its key role is to protect it from external mechanical, chemical and biological insults including pathogens like viruses [32]. Given the fact that the SARS-CoV-2 virus attaches first to mucosal tissues in an individual's airway, it is interesting to note that the surface of mucosal tissues (as opposed to the skin) is coated by non-keratinized epithelium. The multifunctional nature of the glycoprotein mucin which is the main macromolecular component of the mucus allows various types of interactions, as reflected by its structure and unique chemistry. The central core of the mucin molecule is thiol-rich and contains both hydrophobic and charged hydrophilic domains. The majority of mucin structure are

carbohydrates (~80%), which allow high adsorption rates of water and the formation of a hydrogel [33]. Mucin displays a net negative charge owing to the presence of sialic acid residues [34] and thus, it interacts electrostatically with positively charged nanoparticulate matter. Moreover, the ACE2 receptors are expressed in the airway epithelia cells, and it was observed that the receptor is upregulated at the small airway epithelia by smoking, especially in men [35,36]. In other words, the S protein is a fundamental player in the interaction and penetration of virus with the mucus layer prior to its binding to the ACE2 receptor. In a similar way, the S protein and especially the S1 subunit mediates the interaction with fomites.

Protein adsorption onto solid and biological surfaces has been a hot topic in the biomedical field for decades. In particular, protein adsorption is a key step in the foreign-body response to implants in the extra-cardiovascular and cardiovascular systems [37] and various methods have been used to elucidate the mechanisms of attachment, the protein orientation on the surface, the conformational changes that take place at the surface, and the adsorbed amount [38–40]. Fig. 1B shows a 3D representation of hydrophilic and hydrophobic amino acids on the surface of the S protein of SARS-CoV-2, a distribution that most probably contributes to the formation of nonspecific interactions with the environment, including fomites and biological surfaces.

Characterization of the interaction of S1 and S2 subunits of the S protein of SARS-CoV-2 with different chemically modified surfaces is an essential stage in understanding the adsorption process of the virus to surfaces of different nature, and thus calls for the use of facile, easily accessible, and reproducible techniques. The Quartz Crystal Microbalance (QCM) system comprises a disc-shaped quartz crystal that measures the deposited mass on the surface via the difference in resonant frequency of the quartz during the experiment [38–41]. It is a recognized

research tool in surface engineering [41,42], biophysics [46], biomaterials science [44,45,48], and electrochemistry [43,49,50]. A striking advantage of this method is that the surface of the crystal can be coated with materials displaying a broad spectrum of homogenous properties. Meaning, we can control the surface properties and examine each type of possible interaction separately. Therefore, it can be a very useful tool to study the binding of various proteins for purposes such as disease diagnosis [51], detection of DNA mutations by using protein adsorption onto mutated DNA [52], as well as to study the interaction between proteins and specific antibodies [53], etc.

In this work, we utilized dissipation monitoring QCM (QCM-D) to comparatively characterize the adsorption of the SARS-CoV-2 S protein subunits S1 and S2 of the original strain and the S1 subunit of two more transmissible variants, namely Delta (S1-δ) and Omicron (S1-o), to gold-coated QCM-D sensor surfaces modified with various functionalized self-assembled monolayers (SAMs). This comparison allowed us to study the preferable adsorption of the S protein domains, under different pH conditions to various surface chemistries. Overall, the results of this research provide an important insight into the mechanism of SARS-CoV-2 binding to surfaces displaying different features.

2. Results

To investigate the affinities of the SARS-CoV-2 S protein to various surface functionalities, we chose to modify the gold-coated quartz crystals employed in the QCM-D with alkanethiols bearing different functional end-groups. Following overnight immersion of the gold-coated sensors in a dilute solution of alkanethiol in ethanol we qualitatively studied, via water contact angle measurements, the formation of the various SAMs on the surface compared to the bare gold surface as a control. Each differently functionalized SAM produced a surface with a specific chemistry, as observed by the degree of hydrophilicity/hydrophobicity obtained at the surface. Table 1 summarizes the water contact angle values of the variously functionalized surfaces. The contact angles are in a good agreement with those reported in previous works [54–59].

Next, we integrated the chemically modified sensors to study the adsorption of the S1 and S2 proteins. The experiments were performed utilizing the QCM-D tool, while keeping a constant protein concentration of 0.05 mg mL^{-1}. Fig. 2 presents data on the frequency and dissipation shifts collected during the adsorption process. Upon addition of the protein solution, we observed a sudden drop in the frequency values, accompanied by an increase in dissipation. The greater the amount of protein adsorbed, the more pronounced the decrease in frequency. As a final step, we rinsed the sensor surface with protein-free phosphate buffer saline (PBS) for 30 min. This rinsing caused a small increase in the frequency and a small decrease in dissipation owing to detachment of unbound protein molecules. As can be observed from Fig. 2, the frequency and dissipation values did not revert to those observed prior to protein addition. This served as a proof that most of the adsorbed protein remained tightly bound to the sensors surfaces.

Fig. 2 shows that each protein/SAM combination resulted in a different curve behavior, indicating distinct proteins affinity. In the case of the S1 protein, all surface modifications demonstrated a drop in frequency greater than that of the 11A1U-functionalized surface. In

particular, the strongest decrease in frequency was observed for the FOT and 11MUN surface modifications, while the frequency drop was intermediate for 11M1U, TDT and bare gold. In all of these cases, except for 11MUN and 11A1U SAMs, the dissipation was rather high (Fig. 2B).

One distinctive feature of SARS-CoV-2 has been the very high rate of mutation at amino acid residues in the RBD of the S1 subunit that binds the ACE2 receptor in the host cell among variants which strongly affects transmissibility and helps the virus to escape antibody binding [60,61]. For a more detailed description of the fundamental mutations in the S1 subunit readers are referred to Kumar et al. [62] These mutations are anticipated to also change the interaction of the virus with fomites. In this framework, we characterized the adsorption of the S1 subunit of wild type of the virus to that of variants δ and o.

Interestingly, a comparison of the S1 subunit (wild type) to that of the δ- and o-variants revealed a major decrease in frequency and increase in dissipation in the case of 11MUN SAM compared to other modifications (Fig. 2C,E). Another interesting finding concerning the S1-δ subunit was that the decrease in its frequency was lowest on the surface functionalized with the hydrophilic 11M1U SAM. In addition, in the case of the S1-o subunit, during the last 30 min of the experiment (which included PBS-rinsing) there was no increase in the frequency and no decrease in the dissipation, as were observed for both the S1 and the S1-δ subunits (Fig. 3F). This last finding might suggest that binding of the S1-o subunit on the various surfaces was stronger than that of the previous variants, which had exhibited some detachment during the rinsing cycle.

In the case of the S2 subunit, the most significant change in frequency indicated more adsorption to the hydrophobic TDT, while 11A1U and FOT showed the lowest adsorption, as expressed by the lowest frequency changes (Fig. 2G).
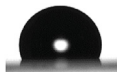
In order to calculate the adsorbed protein mass, we needed to choose the most suitable model. To this end we ascertained whether the attached proteinous surface is thin or thick, rigid or soft. The criterion for thin film is that the Δf (change in frequency during the adsorption process) is less than 2% of the initial resonance frequency [63,64]. In all our experiments this value was less than 0.1%, meaning that we could indeed apply the thin-film model to all of them. In cases where, in addition, the ΔD (dissipation change) was less than 1.5×10^{-6} when the 3$^{\text{rd}}$ overtone was used (n = 3), we utilized the Sauerbrey equation [64] to calculate the mass density of the protein layer adsorbed on the surface. When the ΔD was greater than 1.5×10^{-6}, we calculated the parameters of soft films more accurately by applying the Voigt model.

Fig. 3 presents the calculated mass density of the S1, S1-δ, S1-o and S2 subunits adsorbed onto the various chemically modified sensors.

By comparing the adsorption mass densities of S1 and S1-δ proteins (Fig. 3A), we can establish different affinity trends. In the case of the S1 subunit, the adsorption on the hydrophilic surfaces (11M1U, 11A1U and 11MUN) was favorable compared to that on the hydrophobic TDT SAM. The highest amount was adsorbed onto the surface functionalized with 11MUN (725 ± 25 ng cm^{-2}) (Fig. 3A). In contrast, the S1-δ subunit demonstrated an increase in adsorption to the hydrophobic surfaces (TDT and no-SAM) and a decrease to the hydrophilic ones (11A1U and 11M1U), except for 11MUN, which showed a ~2-fold increase in mass density compared to S1. The latter may also indicate that the adsorbed protein layer was a multilayer [65].

Table 1

Structure of the different self-assembled monolayers (SAMs) used to modify the QCM gold sensor and the static water contact angle after modification. Each value and error were taken as the average and standard deviation (S.D.) of 3–5 measurements, respectively.

SAM	11M1U	11A1U	11MUN	No SAM (bare gold surface)	TDT	FOT
End group	-OH	-NH$_2$	-COOH	–	-CH$_3$	-CF$_3$
Water contact angle ± S.D. (°)	48.0 ± 1.3	55.9 ± 0.5	64.7 ± 1.4	91.6 ± 3.9	110.1 ± 2.1	114.9 ± 1.1
Water drop image						
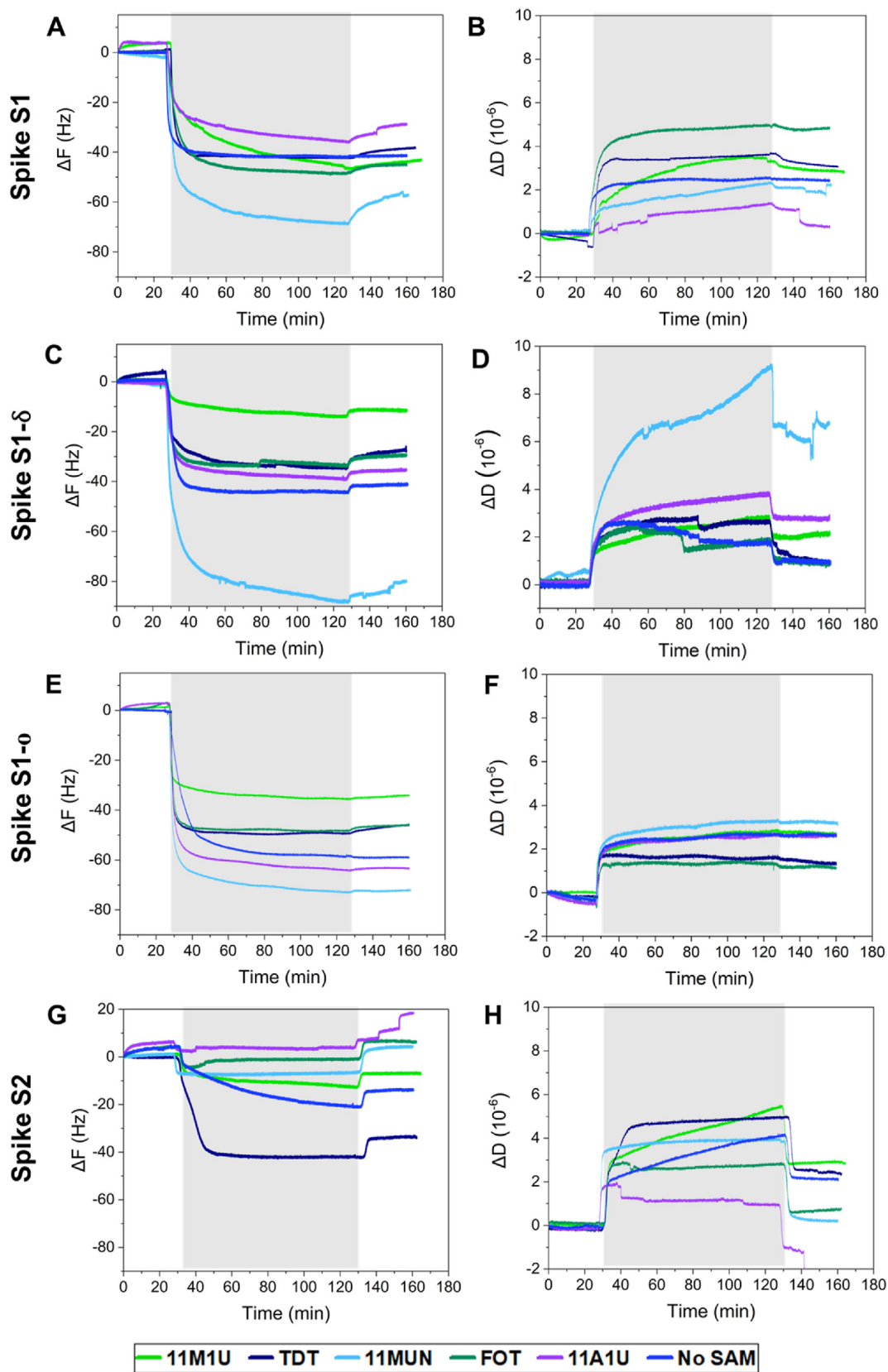
Fig. 2. Representative real time adsorption curves monitored using QCM-D. The frequency and dissipation shifts over time of the S protein subunit S1 (A,B), S1-δ (C,D), S1-o (E,F) and S2 (G,H) on various SAM-functionalized surfaces. The grey background represents the adsorption process of the added proteins (0.05 mg mL^{-1}) and the white background represents protein-free PBS. The 3rd overtone is presented (n = 3).
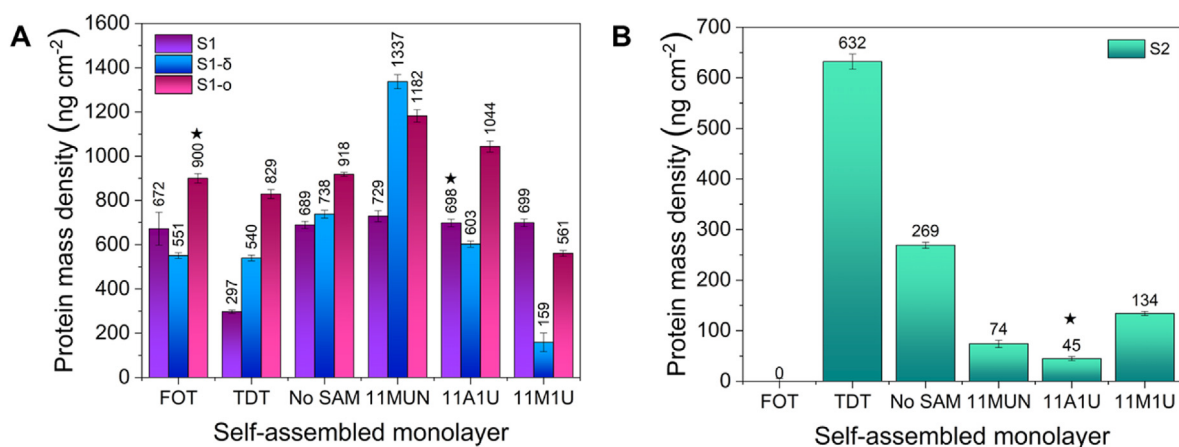
Fig. 3. Calculated average mass density of S1, S1-δ, S1-o (A) and S2 (B) protein layers adsorbed onto various SAM-modified surfaces using Sauerbrey (marked with ★) or Voigt models, n = 3.

The S1-o subunit exhibited the highest adsorption to hydrophobic surfaces (FOT, TDT and bare gold) relatively to all other S1 subunits. Additionally, it was found to adsorb better than the S1-δ subunit onto hydrophilic surfaces (11A1U and 11M1U), but slightly less well than the S1-δ subunit onto the negatively charged 11MUN.

We further calculated the average adsorbed mass density of the proteinous layers formed on all the studied functionalized surfaces in the case of each S1 subunit. From this simple calculation we found that the average mass density and average standard deviation (S.D.) of the S1, S1-δ and S1-o subunits were 631 ± 34, 655 ± 25, and 906 ± 20 ng cm^{-2}, respectively. This result implies that, on average, adsorption of the S1-o subunit on various surfaces was the highest.

In comparing the kinetics of the process of adsorption of each of the S1 subunits onto the 11MUN-functionalized surface during the first 5 min of the adsorption, we calculated that the changes in the frequency (in Hz min^{-1}) over that period were 7 ± 2, 11 ± 1 and 13 ± 2, for the S1, S1-δ and S1-o subunits, respectively. This indicates that while the final mass density on 11MUN SAM was slightly higher for the S1-δ subunit than for the S1-o one, the S1-o subunit adsorption kinetics demonstrated that its interaction with this specific surface was almost 20% faster than that of the S1-δ subunit (although the statistical difference is not significant).

On the TDT-functionalized surface the highest mass density was shown by the S2 subunit, a behavior distinct from all other surfaces. This high mass density correlates with the highest degree in its frequency decrease, as shown in Fig. 3B. The adsorbed mass density of this subunit calculated for all other surface modifications was relatively low (Fig. 3B), especially for FOT-functionalized and 11A1U-functionalized surfaces.

In light of the stronger binding of the S1 subunits to the 11MUN-functionalized surfaces, we further studied this adsorption under different pH conditions. The extracellular pH varies between 7.3 and 7.4 in the case of a healthy person [66], and the pH of the nasal and tracheal mucosa is in the range of 5.3–7 [67] and 6.1–7.9, respectively [68]. Furthermore, smoking or disease such as a common cold, might increase the pH to 8.3, while bacterial infection might reduce the pH to 5.6 [68]. It is of an utmost importance to study the interactions of S1 subunit in these various pH conditions because they can affect its binding to different types of surfaces. Additionally, the rationale for using 11MUN-functionalized surfaces is that it resembles better than any other surface modification in this work the negatively-charged nature of the surface of mucosal tissues that are covered by a layer of mucus and of the ACE2 receptor which are the main interactions of the S protein during viral transmission.

Fig. 4 presents changes in frequency and dissipation at different pH values. Using 0.1 M HCl or NaOH 0.1 M solutions, we adjusted protein-free PBS and protein solution to pH values of 8.5, 7.4, 6.5 and 3. The greatest decrease in the frequency was found in the case of pH 7.4

(Fig. 4A). Interestingly, dissipation was relatively high at pH 6.5, resulting in an adsorbed protein mass as low as that obtained at pH 3 (Fig. 4D), where the decrease in frequency was lowest. Overall, the highest amount of S1 adsorption was observed at pH 7.4, while both the more basic and the more acidic pH conditions inhibited adsorption. In addition, plotting of the change in ΔD as a function of the change in frequency (|Δf|) enabled us to characterize the viscoelastic properties of the protein layers (Fig. 4C).

All the adsorbed protein layers remained relatively rigid for the |Δf| <20, since the slope of the curves (i.e., the change in dissipation) within this range is close to zero. As the protein continued to adsorb, the plots corresponding to pH values 7.4 and 6.5 demonstrated a further increase in slope, indicating that the films were becoming less rigid and more flexible and hydrated, and revealing that at pH 6.5 the protein layer was more viscoelastic than at pH 7.4. The layers formed at pH 8.5 or 3 revealed only a slight increase in slope over time, suggesting that the adsorbed layers can be considered as rigid and dehydrated layers, and hence that the Sauerbrey equation can be reliably applied [68,69].

3. Discussion

Protein adsorption onto surfaces is a complex process that can be affected by several types of interactions (e.g. hydrophobic, electrostatic, ionic) or via hydrogen bonding. Mass and thickness of the adsorbed protein layer are important players in determining the orientation of the proteins on surfaces, and can indicate whether the 3D structure of the protein is preserved or if the protein undergoes denaturation during the process.

As observed from our experiments, the S1 subunits adsorb better onto hydrophilic surfaces such as 11M1U and 11A1U than onto hydrophobic ones. This preferential adsorption can be attributed to the location of the S1 subunit on the periphery of the S protein. With regard to the effect of pH, the S1 subunit adsorbs to a higher extent to the 11MUN SAM surface at a pH of 7.4 than at 3, 6.5 and 8.5. At this pH, the 11MUN SAM functional carboxylic acid end group (pK$_a$ = 5.5–6.0) [71] undergoes deprotonation and becomes negatively charged. It was previously calculated that the isoelectric point (pI) of the RBD of the S1 subunit is > 7.4 [72], and thus most of its surface is positively charged at pH 7.4. This might contribute, by electrostatic interactions, to the strengthening of its adsorption to a negatively charged surface. These results are in line with the fact that the ACE2 receptor which binds RBD is also known to be negatively charged [73]. Moreover, the glycosylated regions in the mucin protein enable intermolecular hydrogen bonding which, under physiological pH conditions, confer a net negative charge due to the presence of ester sulfate (pK$_a$ = 1.0) and sialic acid (pK$_a$ = 2.6) residues that favor electrostatic interactions with positively charged molecules and
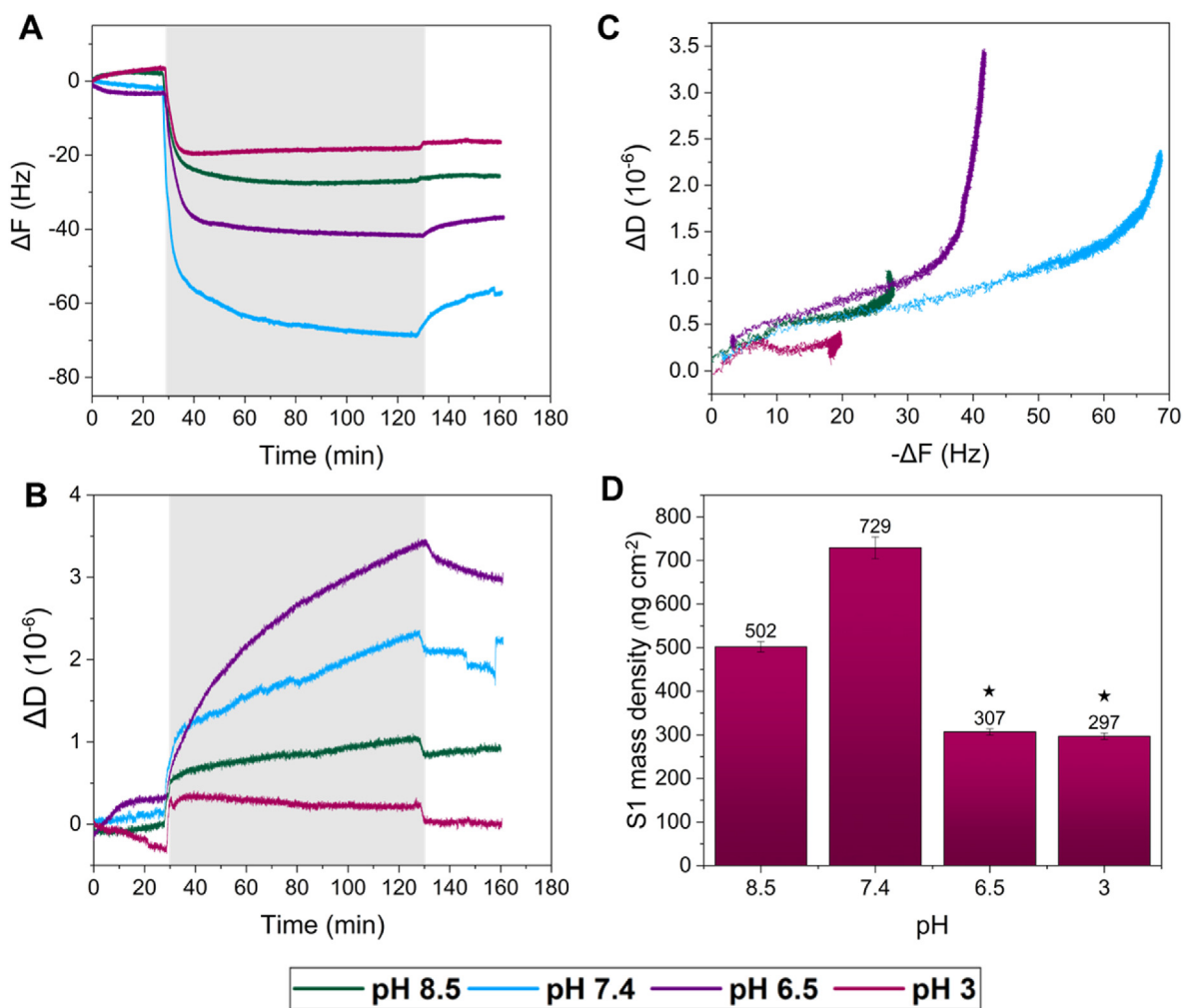
Fig. 4. Representative frequency (A) and dissipation (B) curves (3rd overtone) over time under different pH conditions. The grey background represents the adsorption process of the S1 subunit (0.05 mg mL^{-1}) and the white background corresponds only to the PBS buffer. ΔD *vs.* Δf plot (C). Calculated average mass density of S1 adsorbed layer using Sauerbrey (marked with ★) and Voigt models (D).

particulate matter, including nanostructures such as viruses and nano-pollutants [77]. Indeed, it was proven that SARS-CoV-2 is able to interact with sialic acid via the S1 subunit during the infection process [78,79].

The S1-δ subunit showed a significantly higher capacity for adsorption on 11MUN-functionalized surfaces than that of the original SARS-CoV-2 S1 subunit, and also more than that of S1-o. This can be explained by considering nine of the mutations that developed in the S1-δ protein [74]. Four of these mutations (T19R, L452R, T478K, P681R) [74] exhibited a change from a hydrophobic or uncharged amino acid to a positively charged one (arginine or lysine). Those results suggested that the L452R, T478K and P681R mutations indeed have a significant impact on the increase in viral transmissibility [75], and that this might be the main factor explaining the difference in their adsorption compared to that of the original S1 subunit. In two other mutations, negatively charged amino acids were replaced, one by an uncharged amino acid (D614G) and one was omitted (E156del). For a better understanding of the mutations dispersal in the S1-δ subunit, readers referred to Tian et al. [75] In other words, there was an increase in the positive electrostatic potential of the S1-δ subunit [76]. That increase was probably responsible for the improved ability of this subunit to become adsorbed onto the negatively charged 11MUN-functionalized surface at pH 7.4. This likelihood correlates very well with the reported increase in affinity of the

S1-δ subunit to the negatively charged ACE2 receptor, which probably leads to the higher infection rates than those of the non-mutated S1 subunit [75].

It is a challenging task to understand and predict the influence of the possible mutations potentially present in the S1-o subunit of SARS-CoV-2 on the adsorption behavior on different surfaces. Current mutations in the S1-o subunit probably lead to a 3D structural change and, consequently, in a less effective interaction than that of the original S subunit with the TMPRSS2 (which is abundant in the lungs), and therefore causes a less severe disease [80]. Previous studies showed that the electrostatic potential of the S1-o subunit becomes even more strongly positive than that of the S1-δ subunit, especially in the RBD [81], and this might be one of the reasons for the increase in infection rates caused by the Omicron variant globally. It might be expected that adsorption of the S1-o subunit onto an 11MUN-functionalized surface would be higher than that of the S1-δ subunit, but this is not necessarily the case, and a change in the adsorption capacity might be due to other structural changes caused by the mutations. Previous studies have shown that the affinity of the RBD for the ACE2 receptor from S1-o is weaker than that from S1-δ, and stronger than the one from the original S1 subunit [82,83]. This correlates well with the adsorption rates we obtained using 11MUN. It is important to note that when we consider the average mass density adsorption, the Omicron variant shows the highest overall adsorption

capacity to surfaces displaying different features (e.g., hydrophobicity, charge). This means that the S1-o subunit can create more pronounced chemical bonds with different surfaces, which is more realistic for real-life surfaces.

All S1 subunits also demonstrate capabilities for adsorption onto hydrophobic SAM surfaces such as TDT and FOT, as well as onto the bare gold surface. This observation suggests that during the adsorption process some conformational changes probably occur in the protein: namely, that specific subunit domains become exposed at the surface, and that this can lead to an increase in their adsorption capacity onto hydrophobic substrates. Fig. 1B shows the distribution of hydrophilic and hydrophobic amino acids on the surface of the S protein. Even though the surface of most of the S1 subunit contains hydrophilic amino acids (Fig. 1B - top view), there are also hydrophobic regions that might contribute to this adsorption process onto hydrophobic surfaces. It is interesting to note that in comparison to S1 and S1-δ, S1-o subunits tend to adsorb more successfully to hydrophobic surfaces. It was shown in a previous study that the new mutations increase the hydrophilicity of S1-o RBD, but additionally there are several regions with increased hydrophobicity, which might be an explanation for this behavior [84]. Since the interactions of the protein are not specific as those in the case of binding to the ACE2 receptor, these additional hydrophobic regions might also take part in the interaction with the hydrophobic surfaces. Further analysis is needed in order to study whether these hydrophobic regions are available on the surface. In general, this might suggest that mutations in the S1-o subunits significantly affect the 3D structure and the activity of the S protein.

The length of the whole S protein (vertically to the virus membrane) is ~15 nm [85], and assuming that the S1 and S2 subunits are each about half of this length, we would expect that the monolayer thickness would be approximately 7.5 nm if the orientation of the adsorbed protein is vertical to the surface and closely packed. For the S1 subunit, we observed an adsorbed layer thickness of about 7 nm when using all the sensors, which might suggest that the packing is indeed close, and that the orientation of the protein is almost vertical (Figure S1A) [86,87]. We cannot precisely determine which side of the protein adsorbs onto the sensor, meaning that we cannot establish via this method whether the RBD is oriented towards the surface and interacts with it directly, or is oriented rather towards the outer environment.

On the other hand, there are cases where the thicknesses is smaller (Figure S1A). There are two possible reasons for this: (*i*) low protein density on the surface, leading to non-dense and nonhomogenous packing, or (*ii*) a side-on orientation of the protein on the surface, lowering the thickness of the adsorbed layer. While the first explanation would seem to be more reasonable because of the low mass density, our results can be also explained by a combination of these two phenomena.

The S1-δ and S1-o subunits exhibit significantly thicker layers, of about 14 and 12 nm, respectively, on the 11MUN-functionalized surface than on all other surfaces. S1-o shows relatively high thickness (~10 nm) on 11A1U-functionalizes surface as well. This might indicate the formation of a protein multilayer rather than a ~7.5-nm single protein monolayer.

As can be seen in Fig. 3B, the S2 subunit adsorbed most strongly to the hydrophobic TDT-functionalized surface. This can probably be attributed to its hydrophobic nature, shown in Fig. 1B, and it correlates well with the transmembrane location of the S2 subunit. Usually, the transmembrane portion of the protein is hydrophobic and is not exposed to the outer environment. The interactions of the S2 subunit, therefore, do not contribute to the interactions of the whole S protein with functionalized surfaces and are less significant when compared to TDT, and especially to the possible surface interactions of the different S1 subunits. Specifically, since the S2 subunit is not exposed at the surface of the S protein (Fig. 1A), it is not involved in the interaction of the virus with the environment.

The thickness of the adsorbed proteinous layer on the TDT-functionalized surface was about 6.5 nm (Figure S1B), which might

also suggest a close packing arrangement, since it approximates the full length of the S2 subunit. Substantially lower adsorption was measured on 11A1U- and FOT-functionalized surfaces, and as expected, the thickness of the proteinous layer was close to zero (Fig. 3D). These results are in good agreement with previous reports showing low adhesion of proteins and other macromolecules to perfluorinated surfaces [88]. However, since all S1 subunits, and especially S1-o, demonstrate high affinity to FOT, it indicates that even fluorinated surfaces do not offer a good solution towards inhibiting the attachment of S proteins and reducing the adsorption of the SARS CoV-2 virus.

With regard to the effect of pH, it is known that this factor strongly influences the 3D structure of proteins and their functions. If the pH is altered, with resulting changes to the structure and function of the protein, these conformational changes may be restored when optimal pH conditions are recovered. In some cases, however, the protein undergoes irreversible denaturation. The S protein is stable over a wide range of pH values (3–9), and has been shown to withstand even extreme acidic conditions (pH 2–3) for up to 1 day [27,89,90].

Characterization of a pH-dependent structural conformation of the S protein showed that the pH greatly affects the orientation of the RBD domain [91,92]. It was reported that if the RBD is in an open state (also termed "up state"), it is capable of binding to the ACE2 receptor, whereas in the closed state (also called "down state") such interaction is limited [93–95]. Interestingly, it was proved that the "open state" is better stabilized at the physiological pH of 7.4 (64% − 68%) than at a pH of 6.5 (44% − 46%) or 8 (39% − 41%) [96]. This probably explains our results showing that S1 adsorption is clearly more pronounced at pH 7.4, whereas under either more acidic or more basic conditions there is a decrease in the adsorption level. Since the RBD is positively charged, we can assume that its "open state" allows adsorption in the case where the RBD is oriented toward a negatively charged surface. Reducing or increasing the pH will probably result in a conformational change, as well as a change in the RBD to a "closed state". This might explain the decrease in adsorption onto the 11MUN SAM surface at pH values of 6.5 and 8.5, owing to a less surface-exposed, positively charged RBD.

Another important factor to consider when studying the effect of pH is the pI of the whole S1 subunit within the range of 7.68–8.13 [72], and also that the net charge of the S1 subunit is positive at pH values < pI and negative at pH > pI. Therefore, when comparing the charge of the 11MUN SAM surface and that of the S1 subunit under various pH conditions it is important to understand the role of electrostatic interactions in the adsorption to these surfaces. At pH 3, the carboxylic acid end group of the SAM is protonated, meaning that the surface is neutral, and we can indeed obtain the lowest adsorption of the S1 subunit (297 ± 7 ng cm^{-2}, Fig. 4D). In the range of pH 6.0–7.68, where the S1 subunit is positively charged and the surface is negative, we obtain the highest adsorption specifically at pH 7.4. As a comparison, however, at pH 6.5 the 11MUN carboxylic acid is close to its pK_a value and therefore becomes less negative, and we indeed see a significant decrease in adsorption (307 ± 7 ng cm^{-2}, Fig. 4D). The adsorption mass density at pH 6.5 is similar to that at pH 3, implying that pH values lower than 6.5 do not affect the interaction between the S1 subunit and the surface.

Our results provide strong evidence for the fundamental role of electrostatic interactions in the adsorption of SARS-CoV-2 to surfaces of different nature, including biological ones and, more specifically, to mucosal tissues which play a key role during viral transmission. This, together with our knowledge of the structure and properties of mucus (the outermost layer of every mucosal tissue), is corroborated by the rapid invasion of the respiratory system shown by this virus globally.

4. Conclusions

In this work, using QCM-D, we compared the adsorption behaviors of 4 different proteins (S1, S1-δ, S1-o and S2 subunits originating from SARS-CoV-2) on chemically modified surfaces comprising SAMs with different hydrophobic/hydrophilic characteristics. Comparison of the

adsorption of the S1 subunits from the different strains revealed that they behave differently in the adsorption process. In all S1 subunits the adsorption was highest to the negatively charged 11MUN SAM, but the S1-δ and S1-o subunits showed much higher adsorption than the S1 subunit, probably due to the fact that their positive electrostatic surface charges were higher than those of the original S1 subunit. These findings correlate well with the enhanced transmissibility of the Delta and Omicron variants observed globally.

The S1-o subunit demonstrated the highest capacity for adsorption to the various surfaces, which might corroborate the finding that its transmissibility and probably also its infectivity was the highest among all other variants. The finding that the S2 subunit adsorbed best to the hydrophobic SAM TDT can probably be explained by the fact that this subunit is located inside the membrane, meaning that these hydrophobic interactions do not contribute to the whole S protein interactions with surfaces. The best adsorption of the S1 subunit to 11MUN SAM occurred at pH 7.4, which is the physiological pH, and both more acidic and more basic pH values caused a significant decrease in adsorption. These findings might help us to better understand the process of adsorption onto different surfaces under various pH conditions, and may also be applicable to the process of penetration across mucosal tissues such as the airways and the binding to the ACE2 receptor during infection. Future studies should address the adsorption capacities of whole SARS-CoV-2 viruses to various surfaces and compare the results with those of the current study, which relates to the adsorption capacities of the S protein alone.

Associated content

Experimental part (materials and methods), the difference in the adsorbed layers' thickness.

Credit author statement

Daniela Dobrynin: Performed research and analysis, wrote paper. Iryna Polishchuk: Designed experiments, wrote paper. Lotan Portal: Aided in experiments. Ivan Zlotver: Aided in experiments. Alejandro Sosnik: Wrote paper, developed the concept, attained funding. Boaz Pokroy: Designed experiments, wrote paper, developed the concept, supervised research, attained funding.

Declaration of competing interest

The authors declare that they have no known competing financial interests or personal relationships that could have appeared to influence the work reported in this paper.

Acknowledgment

Appendix A. Supplementary data

Supplementary data to this article can be found online at https://doi.org/10.1016/j.mtbio.2022.100265.

References

[1] F. Li, Structure, function, and evolution of coronavirus spike proteins, Annu. Rev. Virol. 3 (1) (2016) 237–261, https://doi.org/10.1146/annurev-virology-110615-042301.

[2] P. V'kovski, A. Kratzel, S. Steiner, H. Stalder, V. Thiel, Coronavirus biology and replication: implications for SARS-CoV-2, Nat. Rev. Microbiol. 19 (3) (2021) 155–170, https://doi.org/10.1038/s41579-020-00468-6.

[3] C. Huang, Y. Wang, X. Li, L. Ren, J. Zhao, Y. Hu, L. Zhang, G. Fan, J. Xu, X. Gu, Z. Cheng, T. Yu, J. Xia, Y. Wei, W. Wu, X. Xie, W. Yin, H. Li, M. Liu, Y. Xiao, H. Gao, L. Guo, J. Xie, G. Wang, R. Jiang, Z. Gao, Q. Jin, J. Wang, B. Cao, Clinical features of patients infected with 2019 novel coronavirus in wuhan, China, Lancet 395 (10223) (2020) 497–506, https://doi.org/10.1016/S0140-6736(20)30183-5.

[4] J. Fajnzylber, J. Regan, K. Coxen, H. Corry, C. Wong, A. Rosenthal, D. Worrall, F. Giguel, A. Piechocka-Trocha, C. Atyeo, S. Fischinger, A. Chan, K.T. Flaherty, K. Hall, M. Dougan, E.T. Ryan, E. Gillespie, R. Chishti, Y. Li, N. Jilg, D. Hanidziar, R.M. Baron, L. Baden, A.M. Tsibris, K.A. Armstrong, D.R. Kuritzkes, G. Alter, B.D. Walker, X. Yu, J.Z. Li, SARS-CoV-2 viral load is associated with increased disease severity and mortality, Nat. Commun. 11 (1) (2020) 5493, https://doi.org/10.1038/s41467-020-19057-5.

[5] D. Cavanagh, Coronaviridae: a review of coronaviruses and toroviruses, in: Coronaviruses with Special Emphasis on First Insights Concerning SARS, Birkhäuser Basel, Basel, 2005, pp. 1–54, https://doi.org/10.1007/3-7643-7339-3_1.

[6] A. Futerman, The cell biology of SARS-CoV-2, Inference Int. Rev. Sci. 5 (1) (2020), https://doi.org/10.37282/991819.19.79.

[7] L. Zhou, Z. Xu, G.M. Castiglione, U.S. Soiberman, C.G. Eberhart, E.J. Duh, ACE2 and TMPRSS2 are expressed on the human ocular surface, suggesting susceptibility to SARS-CoV-2 infection, Ocul. Surf. 18 (4) (2020) 537–544, https://doi.org/10.1016/j.jtos.2020.06.007.

[8] Y. Huang, C. Yang, X. Xu, W. Xu, S. Liu, Structural and functional properties of SARS-CoV-2 spike protein: potential antivirus drug development for COVID-19, Acta Pharmacol. Sin. 41 (9) (2020) 1141–1149, https://doi.org/10.1038/s41401-020-0485-4.

[9] P. Chambers, C.R. Pringle, A.J. Easton, Heptad repeat sequences are located adjacent to hydrophobic regions in several types of virus fusion glycoproteins, J. Gen. Virol. 71 (12) (1990) 3075–3080, https://doi.org/10.1099/0022-1317-71-12-3075.

[10] S. Matsuyama, N. Nao, K. Shirato, M. Kawase, S. Saito, I. Takayama, N. Nagata, T. Sekizuka, H. Katoh, F. Kato, M. Sakata, M. Tahara, S. Kutsuna, N. Ohmagari, M. Kuroda, T. Suzuki, T. Kageyama, M. Takeda, Enhanced isolation of SARS-CoV-2 by TMPRSS2-expressing cells, Proc. Natl. Acad. Sci. Unit. States Am. 117 (13) (2020) 7001–7003, https://doi.org/10.1073/pnas.2002589117.

[11] M. Hoffmann, H. Kleine-Weber, S. Schroeder, N. Krüger, T. Herrler, S. Erichsen, T.S. Schiergens, G. Herrler, N.-H. Wu, A. Nitsche, M.A. Müller, C. Drosten, S. Pöhlmann, SARS-CoV-2 cell entry depends on ACE2 and TMPRSS2 and is blocked by a clinically proven protease inhibitor, Cell 181 (2) (2020) 271–280, https://doi.org/10.1016/j.cell.2020.02.052, e8.

[12] N.H.L. Leung, Transmissibility and transmission of respiratory viruses, Nat. Rev. Microbiol. 19 (8) (2021) 528–545, https://doi.org/10.1038/s41579-021-00535-6.

[13] J.R.C. Pulliam, C. van Schalkwyk, N. Govender, A. von Gottberg, C. Cohen, M.J. Groome, J. Dushoff, K. Mlisana, H. Moultrie, Increased risk of SARS-CoV-2 reinfection associated with emergence of the Omicron variant in South Africa, medRxiv (2021) 1–43, https://doi.org/10.1101/2021.11.11.21266068.

[14] X. He, W. Hong, X. Pan, G. Lu, X. Wei, SARS-CoV-2 Omicron variant: characteristics and prevention, MedComm 2 (4) (2021) 838–845, https://doi.org/10.1002/mco2.110.

[15] C.C.-19R. Team, SARS-CoV-2 B.1.1.529 (Omicron) variant — United States, december 1–8, 2021, MMWR Morb. Mortal. Wkly. Rep. 70 (50) (2021) 1731–1734, https://doi.org/10.15585/mmwr.mm7050e1.

[16] S. Poudel, A. Ishak, J. Perez-Fernandez, E. Garcia, D.A. León-Figueroa, L. Romaní, D.K. Bonilla-Aldana, A.J. Rodriguez-Morales, Highly mutated SARS-CoV-2 Omicron variant sparks significant concern among global experts – what is known so far? Trav. Med. Infect. Dis. 45 (2022) 102234, https://doi.org/10.1016/j.tmaid.2021.102234.

[17] S.H. Bae, H. Shin, H.-Y. Koo, S.W. Lee, J.M. Yang, D.K. Yon, Asymptomatic transmission of SARS-CoV-2 on evacuation flight, Emerg. Infect. Dis. 26 (11) (2020) 2705–2708, https://doi.org/10.3201/eid2611.203353.

[18] J. Cai, W. Sun, J. Huang, M. Gamber, J. Wu, G. He, Indirect virus transmission in cluster of COVID-19 cases, wenzhou, China, 2020, Emerg. Infect. Dis. 26 (6) (2020) 1343–1345, https://doi.org/10.3201/eid2606.200412.

[19] J.L. Santarpia, D.N. Rivera, V.L. Herrera, M.J. Morwitzer, H.M. Creager, G.W. Santarpia, K.K. Crown, D.M. Brett-Major, E.R. Schnaubelt, M.J. Broadhurst, J.V. Lawler, S.P. Reid, J.J. Lowe, Aerosol and surface contamination of SARS-CoV-2 observed in quarantine and isolation care, Sci. Rep. 10 (1) (2020) 12732, https://doi.org/10.1038/s41598-020-69286-3.

[20] H. Choi, P. Chatterjee, J.D. Coppin, J.A. Martel, M. Hwang, C. Jinadatha, V.K. Sharma, Current understanding of the surface contamination and contact transmission of SARS-CoV-2 in healthcare settings, Environ. Chem. Lett. 19 (3) (2021) 1935–1944, https://doi.org/10.1007/s10311-021-01186-y.

[21] G. Moore, H. Rickard, D. Stevenson, P. Aranega-Bou, J. Pitman, A. Crook, K. Davies, A. Spencer, C. Burton, L. Easterbrook, H.E. Love, S. Summers, S.R. Welch, N. Wand, K.-A. Thompson, T. Pottage, K.S. Richards, J. Dunning, A. Bennett, Detection of

SARS-CoV-2 within the healthcare environment: a multi-centre study conducted during the first wave of the COVID-19 outbreak in england, J. Hosp. Infect. 108 (2021) 189–196, https://doi.org/10.1016/j.jhin.2020.11.024.

[22] M. King, A.M. Wilson, M.H. Weir, M. López-García, J. Proctor, W. Hiwar, A. Khan, L.A. Fletcher, P.A. Sleigh, I. Clifton, S.J. Dancer, M. Wilcox, K.A. Reynolds, C.J. Noakes, Modeling fomite-mediated SARS-CoV-2 exposure through personal protective equipment doffing in a hospital environment, Indoor Air (August) (2021) 1–12, https://doi.org/10.1111/ina.12938.

[23] M. Mohamadi, A. Babington-Ashaye, A. Lefort, A. Flahault, Risks of infection with SARS-CoV-2 due to contaminated surfaces: a scoping review, Int. J. Environ. Res. Publ. Health 18 (21) (2021) 11019, https://doi.org/10.3390/ijerph182111019.

[24] D. Taylor, A.C. Lindsay, J.P. Halcox, Correspondence aerosol and surface stability of SARS-CoV-2 as compared with SARS-CoV-1, Nejm (2010), 0–2.

[25] S. Riddell, S. Goldie, A. Hill, D. Eagles, T.W. Drew, The effect of temperature on persistence of SARS-CoV-2 on common surfaces, Virol. J. 17 (1) (2020) 145, https://doi.org/10.1186/s12985-020-01418-7.

[26] J. Biryukov, J.A. Boydston, R.A. Dunning, J.J. Yeager, S. Wood, A. Ferris, D. Miller, W. Weaver, N.E. Zeitouni, D. Freeburger, P. Dabisch, V. Wahl, M.C. Hevey, L.A. Altamura, SARS-CoV-2 is rapidly inactivated at high temperature, Environ. Chem. Lett. 19 (2) (2021) 1773–1777, https://doi.org/10.1007/s10311-021-01187-x.

[27] H.A. Aboubakr, T.A. Sharafeldin, S.M. Goyal, Stability of SARS-CoV-2 and other coronaviruses in the environment and on common touch surfaces and the influence of climatic conditions: a review, Transbound. Emerg. Dis. 68 (2) (2021) 296–312, https://doi.org/10.1111/tbed.13707.

[28] H. Kitagawa, T. Nomura, T. Nazmul, K. Omori, N. Shigemoto, T. Sakaguchi, H. Ohge, Effectiveness of 222-nm ultraviolet light on disinfecting SARS-CoV-2 surface contamination, Am. J. Infect. Control 49 (3) (2021) 299–301, https://doi.org/10.1016/j.ajic.2020.08.022.

[29] T. Kwon, N.N. Gaudreault, J.A. Richt, Environmental stability of SARS-CoV-2 on different types of surfaces under indoor and seasonal climate conditions, Pathogens 10 (2) (2021) 227, https://doi.org/10.3390/pathogens10020227.

[30] D. Lewis, COVID-19 rarely spreads through surfaces. So why are we still deep cleaning? Nature 590 (7844) (2021) 26–28, https://doi.org/10.1038/d41586-021-00251-4.

[31] E.A. Meyerowitz, A. Richterman, R.T. Gandhi, P.E. Sax, Transmission of sars-cov-2: a review of viral, host, and environmental factors, Ann. Intern. Med. 174 (1) (2021) 69–79, https://doi.org/10.7326/M20-5008.

[32] M. Zanin, P. Baviskar, R. Webster, R. Webby, The interaction between respiratory pathogens and mucus, Cell Host Microbe 19 (2) (2016) 159–168, https://doi.org/10.1016/j.chom.2016.01.001.

[33] G.J. Tortora, Principles of Anatomy and Physiology. *Principles of Anatomy and Physiology*, thirteenth ed., Wiley, Hoboken, N.J, 2011.

[34] S.C. Baos, D.B. Phillips, L. Wildling, T.J. McMaster, M. Berry, Distribution of sialic acids on mucins and gels: a defense mechanism, Biophys. J. 102 (1) (2012) 176–184, https://doi.org/10.1016/j.bpj.2011.08.058.

[35] H. Zhang, M.R. Rostami, P.L. Leopold, J.G. Mezey, S.L. O'Beirne, Y. Strulovici-Barel, R.G. Crystal, Expression of the SARS-CoV-2 ACE2 receptor in the human airway epithelium, Am. J. Respir. Crit. Care Med. 202 (2) (2020) 219–229, https://doi.org/10.1164/rccm.202003-0541OC.

[36] A. Liu, X. Zhang, R. Li, M. Zheng, S. Yang, L. Dai, A. Wu, C. Hu, Y. Huang, M. Xie, Q. Chen, Overexpression of the SARS-CoV-2 receptor ACE2 is induced by cigarette smoke in bronchial and alveolar epithelia, J. Pathol. 253 (1) (2021) 17–30, https://doi.org/10.1002/path.5555.

[37] J.M. Anderson, A. Rodriguez, D.T. Chang, Foreign body reaction to biomaterials, Semin. Immunol. 20 (2) (2008) 86–100, https://doi.org/10.1016/j.smim.2007.11.004.

[38] M. Bellion, L. Santen, H. Mantz, H. Hähl, A. Quinn, A. Nagel, C. Gilow, C. Weitenberg, Y. Schmitt, K. Jacobs, Protein adsorption on tailored substrates: long-range forces and conformational changes, J. Phys. Condens. Matter 20 (40) (2008) 404226, https://doi.org/10.1088/0953-8984/20/40/404226.

[39] M. Wahlgren, T. Arnebrant, I. Lundstöm, The adsorption of lysozyme to hydrophilic silicon oxide surfaces: comparison between experimental data and models for adsorption kinetics, J. Colloid Interface Sci. 175 (2) (1995) 506–514, https://doi.org/10.1006/jcis.1995.1482.

[40] E.A. Vogler, Protein adsorption in three dimensions, Biomaterials 33 (5) (2012) 1201–1237, https://doi.org/10.1016/j.biomaterials.2011.10.059.

[41] X. Huang, Q. Bai, J. Hu, D. Hou, A practical model of quartz crystal microbalance in actual applications, Sensors 17 (8) (2017) 1–9, https://doi.org/10.3390/s17081785.

[42] M.D. Ward, D.A. Buttry, In situ interfacial mass detection with piezoelectric transducers, Science 249 (4972) (1990) 1000–1007, https://doi.org/10.1126/science.249.4972.1000 (80-.).

[43] D.A. Buttry, M.D. Ward, Measurement of interfacial processes at electrode surfaces with the electrochemical quartz crystal microbalance, Chem. Rev. 92 (6) (1992) 1355–1379, https://doi.org/10.1021/cr00014a006.

[44] Z. Lin, R.M. Hill, H.T. Davis, M.D. Ward, Determination of wetting velocities of surfactant supersaders with the quartz crystal microbalance, Langmuir 10 (11) (1994) 4060–4068, https://doi.org/10.1021/la00023a026.

[45] Z. Lin, M.D. Ward, Determination of contact angles and surface tensions with the quartz crystal microbalance, Anal. Chem. 68 (8) (1996) 1285–1291, https://doi.org/10.1021/ac951131z.

[46] F. Wan, T. Nylander, C. Foged, M. Yang, S.G. Baldursdottir, H.M. Nielsen, Qualitative and quantitative analysis of the biophysical interaction of inhaled nanoparticles with pulmonary surfactant by using quartz crystal microbalance with

[47] dissipation monitoring, J. Colloid Interface Sci. 545 (2019) 162–171, https://doi.org/10.1016/j.jcis.2019.02.088.

[48] N.-J. Cho, C.W. Frank, B. Kasemo, F. Höök, Quartz crystal microbalance with dissipation monitoring of supported lipid bilayers on various substrates, Nat. Protoc. 5 (6) (2010) 1096–1106, https://doi.org/10.1038/nprot.2010.65.

[49] P.T. Varineau, D.A. Buttry, Applications of the quartz crystal microbalance to electrochemistry. Measurement of ion and solvent populations in thin films of poly(vinylferrocene) as functions of redox state, J. Phys. Chem. 91 (6) (1987) 1292–1295, https://doi.org/10.1021/j100290a003.

[50] D.A. Buttry, Applications of the QCM to electrochemistry, Electroanal. Chem. A Ser. Adv. 307 (1989) 1–100.

[51] C.H. Lu, Y. Zhang, S.F. Tang, Z. Bin Fang, H.H. Yang, X. Chen, G.N. Chen, Sensing HIV related protein using epitope imprinted hydrophilic polymer coated quartz crystal microbalance, Biosens. Bioelectron. 31 (1) (2012) 439–444, https://doi.org/10.1016/j.bios.2011.11.008.

[52] X. Su, R. Robelek, Y. Wu, G. Wang, W. Knoll, Detection of point mutation and insertion mutations in DNA using a quartz crystal microbalance and MutS, a mismatch binding protein, Anal. Chem. 76 (2) (2004) 489–494, https://doi.org/10.1021/ac035175g.

[53] F. Höök, M. Rodahl, P. Brzezinski, B. Kasemo, Energy dissipation kinetics for protein and antibody-antigen adsorption under shear oscillation on a quartz crystal microbalance, Langmuir 14 (4) (1998) 729–734, https://doi.org/10.1021/la970815u.

[54] A. Friggeri, H. Schönherr, H.J. Van Manen, B.H. Huisman, G.J. Vancso, J. Huskens, F.C.J.M. Van Veggel, D.N. Reinhoudt, Insertion of individual dendrimer molecules into self-assembled monolayers on gold: a mechanistic study, Langmuir 16 (20) (2000) 7757–7763, https://doi.org/10.1021/la000520+.

[55] C. Xu, S. Peng, G. Qiao, X. Zhang, Effects of the molecular structure of a self-assembled monolayer on the formation and morphology of surface nanodroplets, Langmuir 32 (43) (2016) 11197–11202, https://doi.org/10.1021/acs.langmuir.6b02204.

[56] C. Lages, E. Méndez, Contact angle measurements under thermodynamic equilibrium conditions, Anal. Bioanal. Chem. 388 (8) (2007) 1689–1692, https://doi.org/10.1007/s00216-007-1373-1.

[57] Y.J. Jeong, D.-J. Yun, S.H. Noh, C.E. Park, J. Jang, Surface modification of CdSe quantum-dot floating gates for advancing light-erasable organic field-effect transistor memories, ACS Nano 12 (8) (2018) 7701–7709, https://doi.org/10.1021/acsnano.8b01413.

[58] Y. Fujino, R. Nakamura, H.-W. Han, I. Yamashita, T. Shimizu, S. Shingubara, T. Ito, Electrochemical impedance spectroscopy study of liposome adsorption and rupture on self-assembled monolayer: effect of surface charge, J. Electroanal. Chem. 878 (2020) 114572, https://doi.org/10.1016/j.jelechem.2020.114572.

[59] J.D. Bernardin, I. Mudawar, C.B. Walsh, E.I. Franses, Contact angle temperature dependence for water droplets on practical aluminum surfaces, Int. J. Heat Mass Tran. 40 (5) (1997) 1017–1033, https://doi.org/10.1016/0017-9310(96)00184-6.

[60] A. Mittal, A. Khattri, V. Verma, Structural and antigenic variations in the spike protein of emerging SARS-CoV-2 variants, PLoS Pathog. 18 (2) (2022), e1010260, https://doi.org/10.1371/journal.ppat.1010260.

[61] S. Kim, T.T. Nguyen, A.S. Taitt, H. Jhun, H. Park, S.-H. Kim, Y. Kim, E.Y. Song, Y. Lee, H. Yum, K. Shin, Y.K. Choi, C. Song, S.C. Yeom, B. Kim, M. Netea, S. Kim, SARS-CoV-2 Omicron mutation is faster than the chase: multiple mutations on spike/ACE2 interaction residues, Immune Netw. 21 (6) (2021), https://doi.org/10.4110/in.2021.21.e38.

[62] S. Kumar, T.S. Thambiraja, K. Karuppanan, G. Subramaniam, Omicron and Delta variant of SARS-CoV-2: a comparative computational study of spike protein, J. Med. Virol. 94 (4) (2022) 1641–1649, https://doi.org/10.1002/jmv.27526.

[63] N. Fourati, C. Zerrouki, Microbalances à Quartz et Polymères à Empreintes Moléculaires Pour La Détection d'espèces Chimiques. État de l'art de 2010 à 2013, Instrum. Mes. Métrol. 13 (3–4) (2013) 9–37, https://doi.org/10.3166/i2m.13.3-4.9-37.

[64] G. Sauerbrey, Verwendung von Schwingquarzen zur Wägung dünner Schichten und zur Mikrowägung, Z. Phys. 155 (2) (1959) 206–222, https://doi.org/10.1007/BF01337937.

[65] F. You, Q.-H. Shi, Kinetic investigation of protein adsorption into polyelectrolyte brushes by quartz crystal microbalance with dissipation: the implication of the chromatographic mechanism, J. Chromatogr. A 1654 (2021) 462460, https://doi.org/10.1016/j.chroma.2021.462460.

[66] J.R. Casey, S. Grinstein, J. Orlowski, Sensors and regulators of intracellular PH, Nat. Rev. Mol. Cell Biol. 11 (1) (2010) 50–61, https://doi.org/10.1038/nrm2820.

[67] R.J.A. England, J.J. Homer, L.C. Knight, S.R. Ell, Nasal PH measurement: a reliable and repeatable parameter, Clin. Otolaryngol. Allied Sci. 24 (1) (1999) 67–68, https://doi.org/10.1046/j.1365-2273.1999.00223.x.

[68] H. Fischer, J.H. Widdicombe, Mechanisms of acid and base secretion by the airway epithelium, J. Membr. Biol. 211 (3) (2006) 139–150, https://doi.org/10.1007/s00232-006-0861-0.

[69] A.A. Feiler, A. Sahlholm, T. Sandberg, K.D. Caldwell, Adsorption and viscoelastic properties of fractionated mucin (BSM) and bovine serum albumin (BSA) studied with quartz crystal microbalance (QCM-D), J. Colloid Interface Sci. 315 (2) (2007) 475–481, https://doi.org/10.1016/j.jcis.2007.07.029.

[71] K. Sugihara, T. Teranishi, K. Shimazu, K. Uosaki, Structure dependence of the surface pKa of mercaptoundecanoic acid SAM on gold, Electrochemistry 67 (12) (1999) 1172–1174, https://doi.org/10.5796/electrochemistry.67.1172.

[72] F. Krebs, C. Scheller, K. Grove-Heike, L. Pohl, H. Wätzig, Isoelectric point determination by imaged CIEF of commercially available SARS-CoV-2 proteins and the HACE2 receptor, Electrophoresis 42 (6) (2021) 687–692, https://doi.org/10.1002/elps.202100015.

[73] Y. Xie, D. Du, C.B. Karki, W. Guo, A.E. Lopez-Hernandez, S. Sun, B.Y. Juarez, H. Li, J. Wang, L. Li, Revealing the mechanism of SARS-CoV-2 spike protein binding with ACE2, Comput. Sci. Eng. 22 (6) (2020) 21–29, https://doi.org/10.1109/MCSE.2020.3015511.

[74] S. Shiehzadegan, N. Alaghemand, M. Fox, V. Venketaraman, Analysis of the Delta variant B.1.617.2 COVID-19, Clin. Pract. 11 (4) (2021) 778–784, https://doi.org/10.3390/clinpract11040093.

[75] D. Tian, Y. Sun, J. Zhou, Q. Ye, The global epidemic of the SARS-CoV-2 Delta variant, key spike mutations and immune escape, Front. Immunol. 12 (November) (2021) 1–7, https://doi.org/10.3389/fimmu.2021.751778.

[76] S. Pascarella, M. Ciccozzi, D. Zella, M. Bianchi, F. Benedetti, D. Benvenuto, F. Broccolo, R. Cauda, A. Caruso, S. Angeletti, M. Giovanetti, A. Cassone, SARS-CoV-2 B.1.617 Indian variants: are electrostatic potential changes responsible for a higher transmission rate? J. Med. Virol. 93 (12) (2021) 6551–6556, https://doi.org/10.1002/jmv.27210.

[77] G. Lafitte, O. Söderman, K. Thuresson, J. Davies, PFG-NMR diffusometry: a tool for investigating the structure and dynamics of noncommercial purified pig gastric mucin in a wide range of concentrations, Biopolymers 86 (2) (2007) 165–175, https://doi.org/10.1002/bip.20717.

[78] L. Bò, M. Miotto, L. Di Rienzo, E. Milanetti, G. Ruocco, Exploring the association between sialic acid and SARS-CoV-2 spike protein through a molecular dynamics-based approach, Front. Med. Technol. 2 (January) (2021) 1–10, https://doi.org/10.3389/fmedt.2020.614652.

[79] X.L. Sun, The role of cell surface sialic acids for SARS-CoV-2 infection, Glycobiology 31 (10) (2021) 1245–1253, https://doi.org/10.1093/glycob/cwab032.

[80] H. Zhao, L. Lu, Z. Peng, L.-L. Chen, X. Meng, C. Zhang, J.D. Ip, W.-M. Chan, A.W.-H. Chu, K.-H. Chan, D.-Y. Jin, H. Chen, K.-Y. Yuen, K.K.-W. To, SARS-CoV-2 Omicron variant shows less efficient replication and fusion activity when compared with Delta variant in TMPRSS2-expressed cells, Emerg. Microb. Infect. 11 (1) (2022) 277–283, https://doi.org/10.1080/22221751.2021.2023329.

[81] S. Pascarella, M. Ciccozzi, M. Bianchi, D. Benvenuto, R. Cauda, A. Cassone, The electrostatic potential of the Omicron variant spike is higher than in Delta and delta-plus variants: a hint to higher transmissibility? J. Med. Virol. (2021) 1–4, https://doi.org/10.1002/jmv.27528.

[82] C.S. Lupala, Y. Ye, H. Chen, X. Su, H. Liu, Mutations on RBD of SARS-CoV-2 Omicron variant result in stronger binding to human ACE2 receptor, Biochem. Biophys. Res. Commun. 590 (January) (2022) 34–41, https://doi.org/10.1016/j.bbrc.2021.12.079.

[83] L. Wu, L. Zhou, M. Mo, T. Liu, C. Wu, C. Gong, K. Lu, L. Gong, W. Zhu, Z. Xu, SARS-CoV-2 Omicron RBD shows weaker binding affinity than the currently dominant Delta variant to human ACE2, Signal Transduct. Targeted Ther. 7 (1) (2022) 8, https://doi.org/10.1038/s41392-021-00863-2.

[84] B. Li, X. Lu, K.M. McAndrews, R. Kalluri, Mutations in the spike RBD of SARS-CoV-2 Omicron variant may increase infectivity without dramatically altering the efficacy of current multi-dosage vaccinations, bioRxiv (2021), 2021.12.08.471688.

[85] Z. Ke, J. Oton, K. Qu, M. Cortese, V. Zila, L. McKeane, T. Nakane, J. Zivanov, C.J. Neufeldt, B. Cerikan, J.M. Lu, J. Peukes, X. Xiong, H.-G. Kräusslich, S.H.W. Scheres, R. Bartenschlager, J.A.G. Briggs, Structures and distributions of SARS-CoV-2 spike proteins on intact virions, Nature 588 (7838) (2020) 498–502, https://doi.org/10.1038/s41586-020-2665-2.

[86] P. Hampitak, D. Melendrez, M. Iliut, M. Fresquet, N. Parsons, B. Spencer, T.A. Jowitt, A. Vijayaraghavan, Protein interactions and conformations on graphene-based materials mapped using quartz-crystal microbalance with dissipation monitoring (QCM-D), Carbon N. Y. 165 (2020) 317–327, https://doi.org/10.1016/j.carbon.2020.04.093.

[87] K. Xu, M.M. Ouberai, M.E. Welland, A comprehensive study of lysozyme adsorption using dual polarization interferometry and quartz crystal microbalance with dissipation, Biomaterials 34 (5) (2013) 1461–1470, https://doi.org/10.1016/j.biomaterials.2012.10.078.

[88] D.W. Grainger, C.W. Stewart, Fluorinated coatings and films: motivation and significance, ACS (Am. Chem. Soc.) Symp. Ser. 787 (2001) 1–14, https://doi.org/10.1021/bk-2001-0787.ch001.

[89] K.-H. Chan, S. Sridhar, R.R. Zhang, H. Chu, A.-F. Fung, G. Chan, J.-W. Chan, K.-W. To, I.-N. Hung, V.-C. Cheng, K.-Y. Yuen, Factors affecting stability and infectivity of SARS-CoV-2, J. Hosp. Infect. 106 (2) (2020) 226–231, https://doi.org/10.1016/j.jhin.2020.07.009.

[90] M.J. Fumagalli, C.F. Capato, L.A. de Castro-Jorge, W.M. de Souza, E. Arruda, L.T.M. Figueiredo, Stability of SARS-CoV-2 and other airborne viruses under different stress conditions, Arch. Virol. (2021), https://doi.org/10.1007/s00705-021-05293-7. No. 0123456789.

[91] T. Zhou, Y. Tsybovsky, J. Gorman, M. Rapp, G. Cerutti, G.-Y. Chuang, P.S. Katsamba, J.M. Sampson, A. Schön, J. Bimela, J.C. Boyington, A. Nazzari, A.S. Olia, W. Shi, M. Sastry, T. Stephens, J. Stuckey, I.-T. Teng, P. Wang, S. Wang, B. Zhang, R.A. Friesner, D.D. Ho, J.R. Mascola, L. Shapiro, P.D. Kwong, Cryo-EM structures of SARS-CoV-2 spike without and with ACE2 reveal a PH-dependent switch to mediate endosomal positioning of receptor-binding domains, Cell Host Microbe 28 (6) (2020) 867–879, https://doi.org/10.1016/j.chom.2020.11.004, e5.

[92] T. Zhou, Y. Tsybovsky, A.S. Olia, J. Gorman, M.A. Rapp, G. Cerutti, P.S. Katsamba, A. Nazzari, A. Schon, P.D. Wang, J. Bimela, W. Shi, I.-T. Teng, B. Zhang, J.C. Boyington, G.-Y. Chuang, J.M. Sampson, M. Sastry, T. Stephens, J. Stuckey, S. Wang, R.A. Friesner, D.D. Ho, J.R. Mascola, L. Shapiro, P.D. Kwong, A PH-dependent switch mediates conformational masking of SARS-CoV-2 spike, bioRxiv Prepr. Serv. Biol. (2020), https://doi.org/10.1101/2020.07.04.187989.

[93] A.C. Walls, Y.-J. Park, M.A. Tortorici, A. Wall, A.T. McGuire, D. Veesler, Structure, function, and antigenicity of the SARS-CoV-2 spike glycoprotein, Cell 181 (2) (2020) 281–292, https://doi.org/10.1016/j.cell.2020.02.058, e6.

[94] M. Gur, E. Taka, S.Z. Yilmaz, C. Kilinc, U. Aktas, M. Golcuk, Conformational transition of SARS-CoV-2 spike glycoprotein between its closed and open states, J. Chem. Phys. 153 (7) (2020) 075101, https://doi.org/10.1063/5.0011141.

[95] Y. Cai, J. Zhang, T. Xiao, H. Peng, S.M. Sterling, R.M. Walsh, S. Rawson, S. Rits-Volloch, B. Chen, Distinct conformational states of SARS-CoV-2 spike protein, Science (80-.) 369 (6511) (2020) 1586–1592, https://doi.org/10.1126/science.abd4251.

[96] I. Pramanick, N. Sengupta, S. Mishra, S. Pandey, N. Girish, A. Das, S. Dutta, Conformational flexibility and structural variability of SARS-CoV2 S protein, Structure 29 (8) (2021) 834–845, https://doi.org/10.1016/j.str.2021.04.006, e5.